Structure Determination and Analysis of Human Neutrophil Collagenase Complexed with a Hydroxamate Inhibitor†,‡

Frank Grams,§ Mike Crimmin,|| Laurie Hinnes,|| Philip Huxley,*,|| Michael Pieper,⊥ Harald Tschesche,⊥ and Wolfram Bode*,§

Abteilung für Strukturforschung, Max-Planck-Institut für Biochemie, D-82152 Martinsried, Germany, British Biotech Pharmaceuticals Ltd., Watlington Road, Oxford OX4 5LY, U.K., and Fakultät für Chemie und Biochemie, Universität Bielefeld, D-33501 Bielefeld, Germany

Received May 30, 1995; Revised Manuscript Received August 18, 1995⊗

ABSTRACT: Matrix metalloproteinases are a family of zinc endopeptidases involved in tissue remodeling. They have been implicated in various disease processes including metastasis, joint destruction, and neurodegeneration. Human neutrophil collagenase (HNC, MMP-8) represents one of the three "interstitial" collagenases that cleave triple-helical collagens types I, II, and III. Its 163-residue catalytic domain (Met80 to Gly242) has been expressed in *Escherichia coli* and crystallized as a noncovalent complex with the hydroxamate inhibitor batimastat. The crystal structure, refined to 2.1 Å, demonstrates that batimastat binds to the S1−S2′ sites and coordinates to the catalytic zinc in a bidentate manner via the hydroxyl and carbonyl oxygens of the hydroxamate group. The batimastat−collagenase complex is described in detail, and the activities of batimastat analogues are discussed in the light of the protein−inhibitor interactions revealed by the crystallography studies.

Zinc-dependent peptidases play a key role in the biosynthesis and metabolism of a number of bioactive peptides, and inhibitors of these enzymes have long been a target for medicinal chemists. The first zinc peptidase targeted for drug discovery was the angiotensin converting enzyme (ACE),[1] which led in 1977 to the discovery of ACE inhibitors which are still widely used for the treatment of hypertension and congestive heart failure (Ondetti et al., 1977). More recently, the zinc peptidase neutral endopeptidase, EC 3.4.24.11, has been the focus of drug discovery programs aimed at finding novel antihypertensive drugs, some of which have reached phase I/II clinical trials (James et al., 1993). The third and most recent group of zinc peptidases which have become the target for drug discovery is the matrix metalloproteinases (MMPs) and in particular the collagenases, stromelysins, and gelatinases. The physiological role of the MMPs is to break down extracellular matrix components to facilitate connective tissue remodeling which occurs during embryonic development, pregnancy, growth, and wound healing. The MMPs are divided into four classes on the basis of sequence homology and substrate specificity. In the normal adult the degenerative potential of MMPs is held in check both by the latency of the secreted enzymes and by the presence of specific [TIMP-1 (Docherty et al., 1985), TIMP-2 (Stetler-Stephenson et al., 1989), and TIMP-3 (Pavloff et al., 1992)] and nonspecific (α_2-macroglobulin) inhibitors. However, in a variety of pathological conditions the balance between activated enzyme and inhibitors is such that net breakdown of connective tissue occurs. Arthritis is characterized by the erosion of articular cartilage in affected joints resulting from proteoglycan and type II collagen breakdown. Stromelysin (Hasty et al., 1990a) and neutrophil (McCachren et al., 1990) collagenase are generally believed to be involved in the destruction process and are thus the focus of efforts to identify novel treatments for arthritis.

Early work with MMP inhibitors focused on efforts to design inhibitors which could be used for the treatment of arthritis. However, in the course of this work it became clear that connective tissue breakdown, mediated by MMP enzymes, is essential for three events in the growth and spread of malignant tumors: (i) the movement of tumor cells across the vascular basement membrane (metastasis), (ii) primary tumor growth which cannot proceed without the breakdown of surrounding connective tissue, and (iii) the penetration of blood vessels into the growing tumor (Brown, 1993). The realization that MMP inhibitors might be able to block these steps and thus offer valuable alternatives to conventional cytotoxic therapies for cancer prompted scientists at British Biotech to investigate the use of MMP inhibitors as anticancer agents. Efforts to identify which of the MMPs are employed by cancer cells to break down matrix barriers have sought to identify activated MMPs in human clinical tissue from malignant tumors taken during primary surgery. These studies have shown that gelatinase is correlated with the progression of colorectal, gastric, and breast cancers (D'Errico et al., 1991). Increased collagenase activity has been demonstrated in gastric carcinomas (Kubocki, 1990) and epidermoid carcinomas of the oral cavity and larynx (Abramson et al., 1975) and in samples of lung carcinoma (Muller et al., 1991). There have been relatively few reports

† This work was supported in part by grants from the SFB 223 of the Universität Bielefeld and the Fonds der Chemischen Industrie to H.T. and from the SFB 207 of the Universität München and the Fonds der Chemischen Industrie to W.B.

‡ Refined model coordinates have been deposited in the Brookhaven Protein Data Bank (file name 1MMB).

* Authors to whom correspondence should be addressed.
§ Max-Planck-Institut für Biochemie.
|| British Biotech Pharmaceuticals Ltd.
⊥ Universität Bielefeld.

⊗ Abstract published in *Advance ACS Abstracts,* October 1, 1995.

[1] Abbreviations: ACE, angiotensin-converting enzyme; HFC, human fibroblast collagenase, MMP-1; HNC, human neutrophil collagenase, MMP-8; MMP, matrix metalloprotease; TIMP, tissue inhibitor of metalloproteinase; TLN, thermolysin.

0006-2960/95/0434-14012$09.00/0

Table 1: Previous MMP Structural Studies[a]

protein	inhibitor	binding mode	reference
HFC (P101−S269)	Z-NHCH$_2$CH$_2$CH(COOH)-Leu-Phe-NHCH$_2$CH$_2$-morpholine	substrate-like (P1−P3′)	Lovejoy et al. (1994)
HFC (V95−P275)	HONHCOCH$_2$CH(iBu)CO-Leu-Ala-OEt	substrate-like (P1−P3′)	Borkakoti et al. (1994)
HFC (N100−S269)	HONHCOCH$_2$CH(iBu)CO-Phe-NMe	substrate-like (P1′−P2′)	Spurlino et al. (1994)
HNC (M80−G242)	Pro-Leu-Gly-NHOH	substrate-like (P3−P1)	Bode et al. (1994)
HNC (F79−G242)	Pro-Leu-Gly-NHOH	substrate-like (P3−P1)	Reinemer et al. (1994)
HNC (M80−G242)	HONHCOCH$_2$CH(iBu)CO-Phe-NMe	substrate-like (P1′−P2′)	Stams et al. (1994)
HNC (M80−G242)	HS-CH$_2$-CH(Bzl)CO-Ala-Gly-NH$_2$	substrate-like (P1′−P2′)	Grams et al. (1995)
HNC (M80−G242)	HONHCOCH(iBu)CO-Ala-Gly-NH$_2$	non-substrate-like	Grams et al. (1995)

[a] Residue 101 in HFC corresponds to residue 80 in HNC.

of stromelysin expression in human tumors, although whether this reflects a lack of involvement in human tumor progression is unclear.

Until recently MMP inhibitor design has relied on a knowledge of the active site derived from crystallographic models of related enzymes such as carboxypeptidase A and thermolysin. Our current medicinal chemistry effort is focused on identifying analogues of batimastat with improved oral activity. In order to provide better structural models to guide this work, we undertook a structural analysis of batimastat (BB-94) bound to truncated neutrophil collagenase. In this paper we describe the three-dimensional structure of the enzyme−ligand complex. The results provide a detailed picture of the key interactions between batimastat and the enzyme active site.

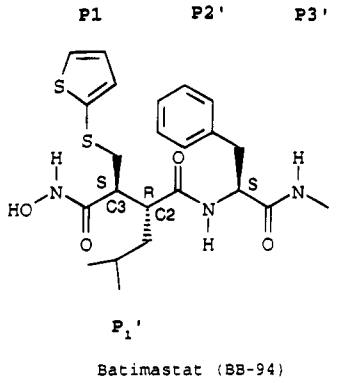

Batimastat (BB-94)

The Discovery of Batimastat. By analogy with the design of ACE inhibitors, the strategy for MMP inhibitor design has been to incorporate scissile bond surrogate functionality into specific pseudopeptide substrates. Chemists working on the discovery of batimastat focused on α-substituted C-terminal analogues containing P1′ and P2′ amino acids and employed the hydroxamate moiety as a scissile bond replacement (Campion et al., 1990). Synthetic work in this area resulted in the discovery of batimastat: 4-(*N*-hydroxyamino)-2(*R*)-isobutyl-3(*S*)-[(2−thienylthiomethyl)succinyl]-L-phenylalanine-*N*-methylamide. Batimastat is a broad spectrum inhibitor with low nanomolar activities against the matrix metalloproteinases (fibroblast collagenase, 3 nM; neutrophil collagenase, 10 nM; stromelysin, 20 nM; 72 kDa gelatinase, 4 nM; 92 kDa gelatinase, 1 nM). In an *in vivo* model with nude mice bearing human ovarian carcinoma xenografts, treatment with batimastat caused resolution of the ascitic disease. Tumor burden was dramatically reduced and survival increased 5−6-fold (Davies et al., 1993). These effects were demonstrated to be due to the matrix metalloproteinase inhibiting effects of batimastat since its inactive diastereoisomer had no effect on tumor biology. More recently, batimastat has shown promising results in a phase I/II clinical trial. A single rising-dose study of intraperitoneal batimastat in patients with malignant ascites has been completed. Following intraperitoneal dosing, plasma levels were maintained in excess of the therapeutic range previously determined in animal models, and batimastat was well tolerated with no significant acute toxicity. Although the primary purpose of the study was to assess safety, pharmacodynamic measures of weight, girth, and time to reaccumulation of ascites were made. Preliminary analysis of these results has been encouraging, and phase III studies with batimastat are planned to commence later this year.

Previous MMP Structural Studies. Most of the X-ray structures of MMP inhibitor complexes published so far show a substrate-like binding of the inhibitor along the active site cleft and a zinc-binding group which is in most cases a hydroxamic acid group (Table 1). With the exception of PLG-NHOH (Bode et al., 1994; Reinemer et al., 1994) the inhibitors are all right-hand-side inhibitors with large hydrophobic P1′ residues occupying the S1′ pocket of the protein. There are no real S2′ or S3′ pockets. In all cases the P2′ residue sits in a cleft formed on the upper side by residues Gly158 and Ile159 and on the lower side by residues Pro217 and Asn218 [residues and residue numbers refer to the pro HNC nomenclature (Hasty et al., 1990b)]. The P3′ residue is mainly exposed to solvent. The left-hand-side inhibitor, PLG-NHOH, sits in a large shallow S2 subsite and a more invaginated S3 subsite, which is ideally shaped to accommodate the P3 proline residue (Bode et al., 1994; Reinemer et al., 1994).

MATERIALS AND METHODS

Purification of the Protein. The Met80−Gly242 catalytic domain of human HNC was expressed in *Escherichia coli* and renatured by dialyzing the inclusion bodies, which were solubilized in 6 M urea and 100 mM β-mercaptoethanol, against a buffer containing 100 mM NaCl, 5 mM $CaCl_2$, 0.5 mM $ZnCl_2$, and 20 mM Tris-HCl, pH 7.5, as previously described (Schnierer et al., 1993). The renatured enzyme was subsequently purified to apparent homogeneity by hydroxamate affinity chromatography as judged by SDS−PAGE.

Synthesis of the Inhibitors. Batimastat was synthesized following the method described by Campion et al. (1990), and compounds **2**−**8** were prepared by analogous methods.

Enzyme Assays. The HFC assay was performed using ^{14}C-acetylated collagen (Cawston & Barrett, 1979). The HNC assay used the fluorogenic substrate Dnp-Pro-Leu-Gly-Leu-Trp-Ala-D-Arg-NH$_2$ (Stack & Gray, 1989), following standard procedures (Grams, 1995).

Table 2: Data Collection Statistics

no. of measurements	33465
no. of observations	32085
no. of unique reflections ($I/\sigma(I) > 0$)	9465
completeness of data (%)	
∞−2.1 Å	89.1
2.20−2.15 Å	91.5
2.15−2.10 Å	34.8
R_{merge}[a]	0.103
R_{sym}[b]	0.048
cell constants a, b, c (Å) ($\alpha, \beta, \gamma = 90°$)	33.67, 69.64, 73.40

[a] $R_{merge} = \sum_h\sum_i(|I(h,i) - \langle I(h)\rangle|)/\sum_h\sum_i I(h,i)$, where $I(h,i)$ is the intensity value of the ith measurement of h and $\langle I(h)\rangle$ is the corresponding mean value of h for all i measurements of h; the summation is over all measurements. [b] $R_{sym} = \sum(|I_F - \langle I_F\rangle|)/\sum I_F$, where I_F is the averaged value of point group related reflections and $\langle I_F\rangle$ is the averaged value of a Bijvoet pair.

Crystallization. Crystallization was performed by hanging drop vapor diffusion at 22 °C. Droplets were made by mixing 2 μL of an 8 mg/mL HNC solution in 3 mM Mes/NaOH, 100 mM NaCl, 5 mM $CaCl_2$, and 0.02% NaN_3 at pH 6.0 and 6 μL of batimastat/PEG 6000 solution. The latter solution was prepared by mixing 10% m/v PEG 6000 in 0.2 M Mes/NaOH at pH 6.0 with ca. 0.5 mg/L batimastat. The resulting suspension was centrifuged, and the supernatant was used for crystallization. The droplets were concentrated against a reservoir buffer consisting of 0.8 M potassium phosphate buffer and 0.02% NaN_3 at pH 6.0. A crystal of 0.50 × 0.45 × 0.04 mm size was obtained within 2 weeks and harvested into buffer made from 15 μL of 20% (m/v) PEG 6000, 0.5 M NaCl, 0.1 M $CaCl_2$, 0.1 M Mes/NaOH, 0.02% NaN_3, pH 6.0, and 2 μL of ca. 3 mM batimastat in DMF. The crystal belongs to the orthorhombic space group $P2_12_12_1$ and exhibits lattice constants of a = 33.67 Å, b = 69.64 Å, c = 73.40 Å, and $\alpha = \beta = \gamma = 90°$, virtually identical to our other HNC complexes (Bode et al., 1994; Reinemer et al., 1994; Grams et al., 1995). The asymmetric unit contains one monomer.

Structure Analysis. X-ray data to 0.21 Å resolution were collected on a MAR image plate area detector (MAR Research, Hamburg) mounted on a Rigaku rotating anode X-ray generator (Λ = 1.5418 Å, operated at 5.4 kW). X-ray intensities were evaluated with the MOSFLM program package (Leslie, 1991), and all X-ray data were loaded with PROTEIN (Steigmann, 1991). The data collection statistics for the complex are given in Table 2. A $2F_o - F_c$ electron density map was computed using all reflection data (Table 2) and the 2.0 Å model of the Met80−Gly242 form of HNC (Bode et al., 1994) for phasing. The nonpeptidic part of the inhibitor was built with the program InsightII (Insight II, 1993), and the complete inhibitor model was fitted to the electron density map using the interactive graphics program FRODO (Jones, 1978). The resulting complex was subjected to reciprocal space least squares refinement with energy constraints as implemented in X-PLOR version 3.1 (Brünger, 1993) using force-field parameters derived by Engh and Huber (1991). The refined model was compared with the improved density, rebuilt, and refined to convergence. A patch residue including the central zinc and the three surrounding His Nε2 atoms together with both oxygens of the hydroxamic acid was defined for the active site zinc. The other three metals were treated as described previously in the PLG-NHOH structure (Bode et al., 1994). Where appropriate density was present at 1σ contouring in the omit Fourier of and 2σ contouring in difference Fourier maps, 170 water molecules were introduced at stereochemically reasonable positions. In the last refinement step individual temperature factors were refined by applying bonded and angular temperature restraints, as recommended by the X-PLOR protocol. The final R-factor is 0.189. The final refinement statistics of the complex are shown in Table 3.

Table 3: Final Refinement Statistics

resolution range (Å)	8.0−2.1
no. of unique data in resolution range	9282
total no. of protein atoms (excluding hydrogen)	1266
solvent atoms (excluding hydrogens)	170
R-factor[a]	8.0−2.1 Å, 0.189; 2.17−2.10 Å, 0.295
rms deviations from target values (excluding metals and hydrogens)	
bonds (Å)	0.015
angles (deg)	1.9

[a] $R = (\sum|F_o - F_c|)/\sum F_o$.

Molecular Modeling. Molecular modeling was carried out using SYBYL version 6.1 (SYBYL, 1995). The energy calculations were carried out using the Kollman all-atom force field (Weiner et al., 1984) with an 8 Å cutoff and a distance-dependent dielectric. Kollman charges were used for the HNC residues. Charges on the inhibitors were calculated using MOPAC with the AM1 Hamiltonian (Stewart, 1990). A quadratic restraint function with a 20 kcal/(mol·Å^2) force constant was used to constrain the hydroxamate oxygen atoms to within 2.0 ± 0.2 Å of the catalytic zinc. During the minimization the coordinates of the inhibitor and residues within 5.0 Å of the experimental batimastat coordinates were allowed to relax. The remaining residues were held fixed. Energy minimization using the MAXIMIN2 (SYBYL, 1995) minimizer was continued until the rms force on the relaxed atoms was less than 0.05 kcal/(mol·Å).

RESULTS

Principal Features of the Collagenase Catalytic Domain. The detailed topology of HNC has been described elsewhere (Bode et al., 1994; Reinemer et al., 1994), and only principal features of the catalytic domain are summarized here. HNC exhibits a spherical shape, with a shallow active site cleft separating a bigger "upper" N-terminal domain from a smaller "lower" C-terminal domain (see Figure 1, which hearafter defines our standard view). The main upper domain consists of a central highly twisted five-stranded β-pleated sheet and two long α-helices including the active site helix containing the two zinc-binding histidine and catalytic glutamic acid residues of the His197-Glu198-Xaa-Xaa-His201 zinc-binding motif. The key inhibitor and substrate-binding residues in the upper domain comprise residues Leu160−Phe164 of the β4 "edge" strand positioned "above" the active site helix and the preceding "bulged segment" Gly155−Leu160. The "catalytic" zinc ion (Zn999) is situated at the bottom of the active site cleft and is coordinated to the Nε2 imidazole atoms of the three HEXXHXXGXXH histidine residues and the hydroxamic oxygens of the inhibitor.

The small lower domain is less regularly organized. It includes helix C and the topologically conserved 1,4 turn

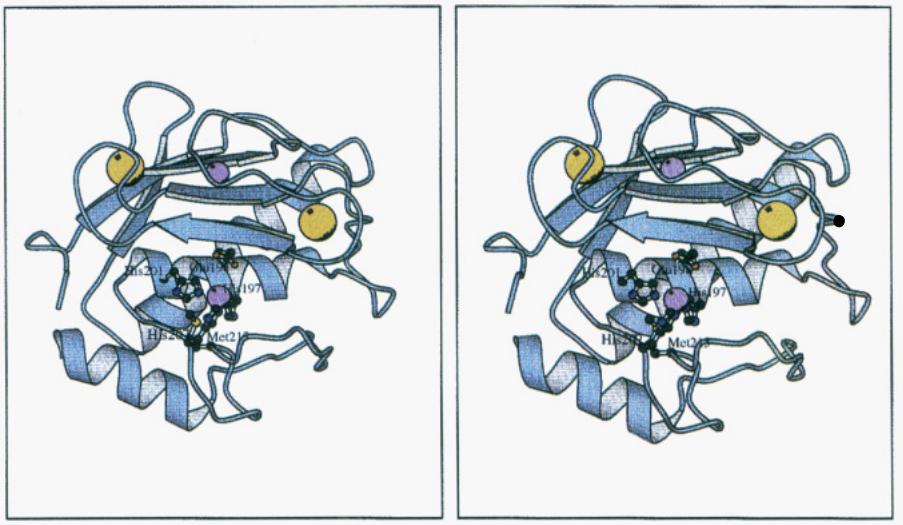

FIGURE 1: Stereo plot of the Met80−Gly242 catalytic domain of HNC (defined from Pro86 onward) shown as a ribbon drawing (using the program Molscript).

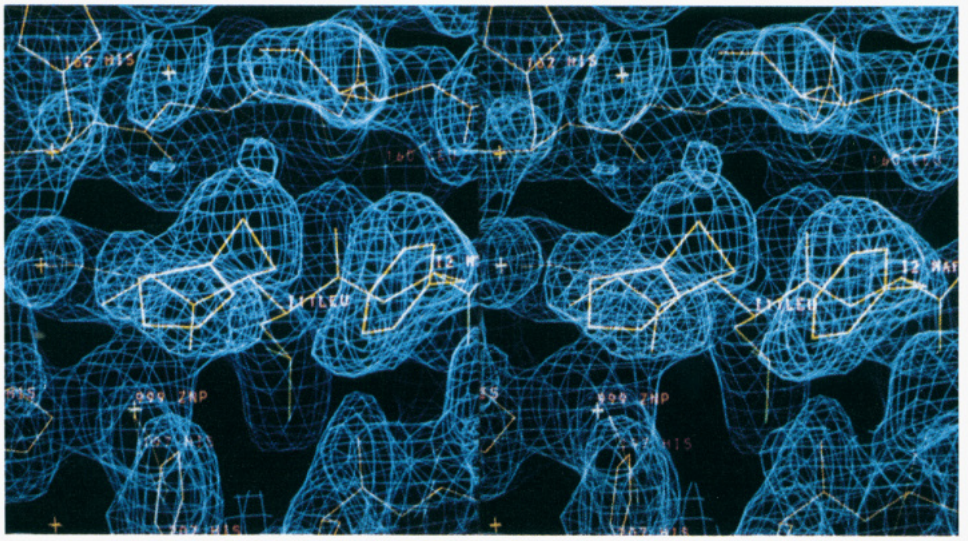

FIGURE 2: Stereo plot of the final $2F_o - F_c$ electron density around batimastat.

from Ala213 to Tyr216, which is characteristic of the "metzincins" (Bode et al., 1993), and provides a hydrophobic base for the three zinc-liganding histidines. At Pro217 the peptide chain kinks and continues in the extended strand Pro217−Tyr219. This "wall-forming" strand separates a long surface crevice from bulk water. The deep S1′ pocket created invaginates immediately to the right of the catalytic zinc. The mouth of this pocket is formed by the three bulge-edge residues Ile159, Leu160, and Ala161, the side chain of Val194 in the active site helix, the wall-forming residues Tyr216, Pro217, and Asn218, and the side of the zinc-binding His197 imidazole ring. The interior of the pocket is formed by the side chains of residues Tyr219−Tyr227, Leu214−Ala213, and Leu193. The bottom of the HNC S1′ pocket is largely blocked by the long side chain of Arg222, flanked on either side by the side chains of Leu193 and Leu214.

Interactions of Batimastat with Neutrophil Collagenase. Figure 2 shows a section around the bound inhibitor of the complex formed by batimastat and HNC. There is clear density showing the inhibitor binding to the primed subsites of the catalytic domain. Batimastat coordinates the catalytic zinc in a bidentate manner via the hydroxyl and the carbonyl oxygen of the hydroxamic group in a fashion similar to that of other hydroxamate inhibitors. Both hydroxamate oxygens, together with the three liganding histidine nitrogens of the enzyme, make up a trigonal-bipyramidal coordination sphere around the catalytic zinc. The hydroxamate group forms additional interactions with the enzyme via the hydroxy group and the nitrogen atom which are within hydrogen-bonding distance of the Glu198 carboxylate and Ala161 carbonyl groups, respectively (Table 4).

Table 4: Selected Hydrogen-Bonding and Zinc-Binding Distances

inhibitor	enzyme	distance (Å)
hydroxamate CO	Zn	1.96
hydroxamate OH	Zn	2.30
hydroxamate OH	Glu198 OE1	2.76
hydroxamate NH	Glu198 OE2	3.25
hydroxamate NH	Ala161 O	3.14
Leu O	Leu160 N	2.80
Phe N	Pro217 O	3.17
Phe O	Tyr219 N	2.89
P3′ N	Gly158 O	2.97

The "peptide backbone" of the inhibitor is bound in an overall extended manner ($\Phi I1 = -177.5$, $\Psi I1 = 121.7$, $\Phi I2 = -105.4$, $\Psi I2 = 144.0$). It lies antiparallel to the bulge-edge strand Gly158−Ala161 and parallel to the Pro217−

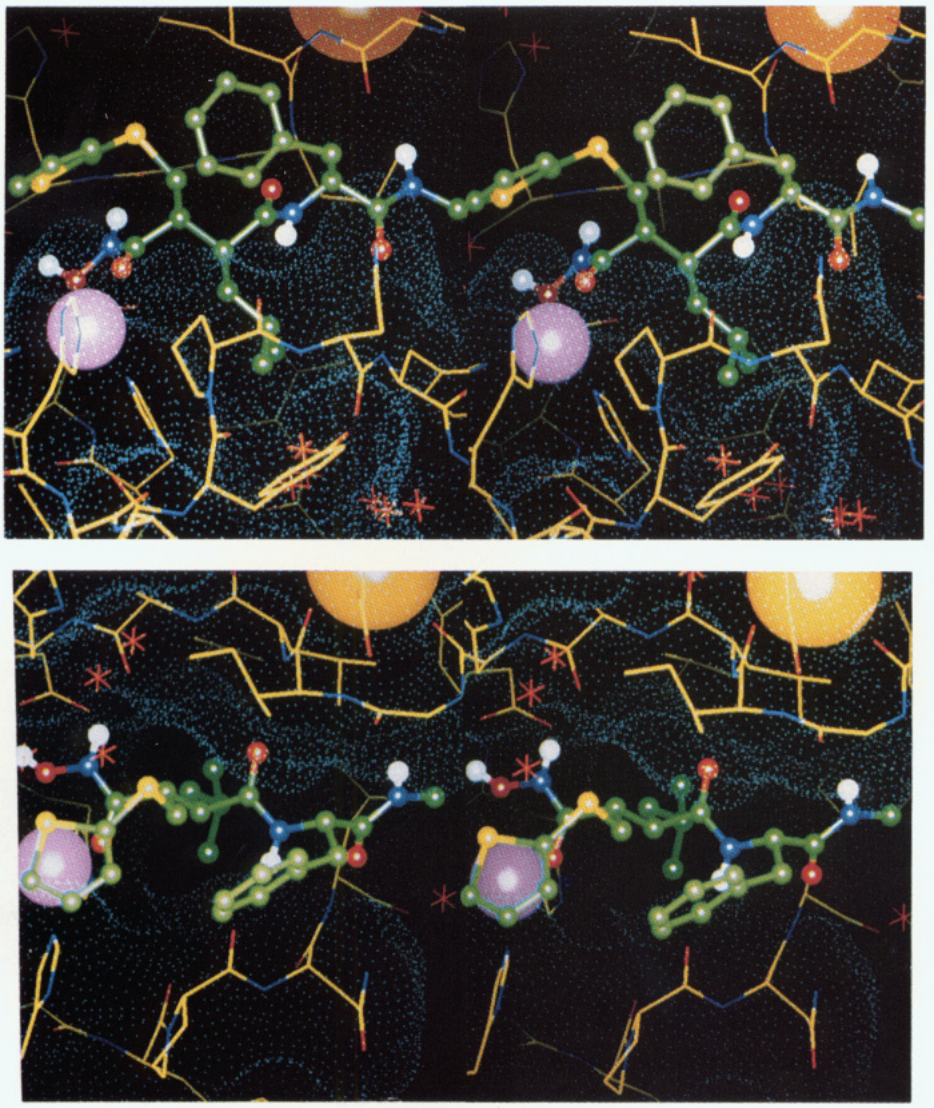

FIGURE 3: (a, top) Detailed view of the batimastat−HNC active site complex. Shown are the edge-strand (β4) residues Gly158−His162, the zinc-coordinating residues His197 and His207, the wall-forming strand residues Pro217−Asn218, batimastat (green), the catalytic zinc ion (Zn999, magenta sphere), one of the calcium ions (Ca997, yellow sphere), localized solvent molecules (asterisks), and the overlayed Connolly dot surface. (b, bottom) Detailed view of the batimastat−HNC complex viewed from above. Shown are the edge-strand (β4) residues Ile159−Ala161, the zinc-coordinating residue His207, the catalytically important glutamate residue Glu198, the wall-forming strand residues Pro217−Asn218, batimastat (green), the catalytic zinc ion (Zn999, magenta sphere), one of the calcium ions (Ca997, yellow sphere), localized solvent molecules (asterisks), and the overlayed Connolly dot surface.

Tyr219 segment on the other side of the active site cleft (Table 4, Figures 3 and 4).

The plane of the thiophene ring is clearly defined by electron density, but Fourier and difference Fourier maps were unable to distinguish between two possible ring conformations. In the conformation shown in Figure 3 the sulfur atom hydrogen bonds via a water molecule to the carbonyl oxygen of Ala163 and is within hydrogen-bonding distance of the hydroxyl oxygen and nitrogen atoms of the hydroxamate group. In the second conformation, the sulfur atom points toward the surrounding solvent away from the enzyme surface. In both conformations the thiophene ring is located above the zinc atom in a conformation reminiscent of zinc aromate half-sandwich complexes. Although the distance between the zinc and the center of the thiophene ring (4.5 Å) is much greater than that found in crystallographic complexes in the Cambridge Structural Database (2.0−3.0 Å) (Allen & Kennard, 1993), there will be favourable electrostatic interactions between the partial negative charge of the thiophene π orbitals and the positive charge on the catalytic zinc, which will act to stabilize the complex.

The P1′ leucine side chain extends into the S1′ pocket, making hydrophobic contacts with the face of the zinc-liganding His197 imidazole ring, the side of the Pro217−Asn218 amide bond, and the Tyr219 and Val194 side chains. At the bottom of the pocket three localized water molecules are in weak hydrogen bond contact with bulk water molecules. The conformation of the leucine side chain and the many hydrophobic contacts made with the S1′ pocket wall are presumably similar to those observed in substrate−enzyme complexes.

The P2′ phenyl ring on batimastat forms intramolecular contacts with the thiomethyl spacer and the thiophene ring of the inhibitor and intermolecular contacts with the Ile159 side chain and the pyrrolidine and carbonyl groups of Pro217. These interactions give rise to a smooth surface spanning the primed region of the cleft. In the crystal structure the benzene ring is involved in two additional intermolecular atom−atom contacts with the Val129 side chain of a

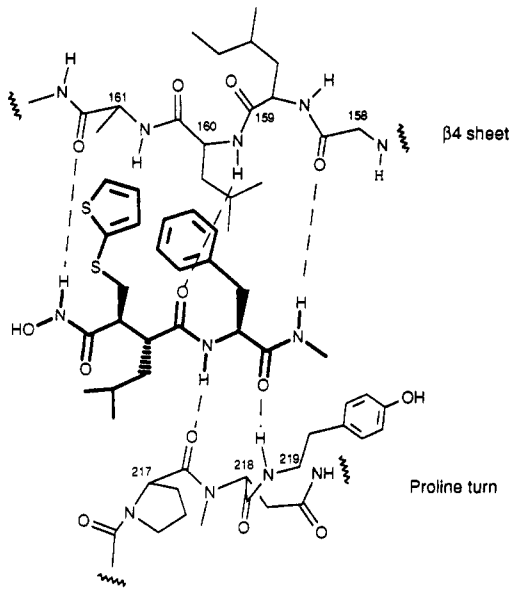

FIGURE 4: Schematic illustration of the batimastat−HNC binding interactions. Hydrogen bonds are shown as dashed lines.

symmetry-related molecule. However, this interaction does not determine the inhibitor Phe side-chain conformation, and modeling experiments show that the crystal packing would allow other conformations of the benzyl side chain. The C-terminal *N*-methyl group points into a shallow water filled pocket, where it is in weak hydrophobic contact with Leu160, Tyr189, and Tyr219.

Chiral Discrimination by the HNC Active Site. It is well-known that enzymes discriminate between the diastereomers of potent inhibitors, and collagenase inhibition by batimastat is no exception to this rule. Its enantiomer, **2**, and diastereomer, **3**, are both inactive at 40 μM (Table 5). However, in both of these structures two or more of the three chiral centers on batimastat are inverted, and they can therefore not be used to probe the role of individual chiral centers in the active site. Structure **4** is a homologue of batimastat, in which a methyl group replaces the P1 2-thienylthiomethyl side chain. In the course of our medicinal chemistry program two diastereomers of **4**, with inverted chirality at C2 (structure **5**) and C3 (structure **6**), were synthesized as active site probes. It can be seen from Table 5 that inversion at either center greatly reduces activity against HFC. In order to understand the enzyme−inhibitor interactions underlying the activity changes accompanying inversion at C2 and C3, we have docked **4**, **5**, and **6** into the active site and analyzed their *in vitro* activities in the light of the modeled complexes. In the discussion that follows, we assume that SAR determined for the inhibition of HFC will parallel that for HNC, since the two active sites are known from crystallographic studies to be almost identical (Bode et al., 1994; Spurlino et al., 1994).

As would be expected from its structure, docking studies demonstrate that **4** can be overlayed almost exactly on the coordinates of batimastat. In structure **5** inversion of stereochemistry at the C2 carbon reduces activity 1000-fold, corresponding to a 4 kcal/mol difference in the free energy of binding between structure **4** and structure **5**. We have docked structure **5** into the active site and energy minimized the resulting coordinates as described in the Materials and Methods section. The coordinates of the phenylalanine side chain, backbone, and hydroxamate group in the modeled complex are similar to those in the batimastat complex. However, the switch from *R* to *S* stereochemistry at the C2 carbon changes the location of the leucine side chain in the S1′ pocket. The P1′ Cα and Cβ atoms are displaced 0.5 Å above and 1.2 Å below the corresponding atoms in the batimastat complex, and the terminal methyl groups are moved toward the Pro217−Asn218 amide bond and away from the Val194 side chain (Figure 5). The cost of adopting the bound conformation is no higher in structure **5** than in structure **4** (it may even be a little lower), and most of the activity loss which accompanies inversion at C2 can be ascribed to intermolecular interactions: less favorable attractive interactions between the P1′ terminal methyl groups and the Val194 side chain; repulsive interactions between the P1′ terminal methyl groups and the Pro217−Asn218 amide bond; and repulsive interactions between the displaced Cβ atom and the Nϵ2 atom of the zinc-binding His197 residue. Inversion at C2 is thus incompatible with optimal van der Waals interactions between the leucine P1′ side chain and the S1′ pocket and results in the loss in activity that is observed with structure **5**.

In structure **6**, changing the C3 stereochemistry from *S* to *R* results in more than a 1000-fold loss in activity, corresponding to a free energy cost of around 4.5 kcal/mol. This dramatic loss in activity is unexpected insofar as the Fourier and Fourier difference maps are only marginally in favor of models with *S* stereochemistry at C3. Modeling studies suggest that both intermolecular and intramolecular interactions contribute to the poor activity of **6**. The C3 methyl group, which points toward solvent in **4**, is directed toward the β4 strand in **6**, giving rise to a large unfavorable interaction (<3.0 Å) between the C3 methyl and the Ala161 carbonyl group (Figure 6). The largest unfavorable intramolecular interaction arises from the close approach of the hydroxamic NH group to the C3 methyl in the bound conformation (<3.0 Å). Neither of these unfavorable interactions occur in the HNC−structure **4** modeled complex, and together they probably account for most of the activity loss which follows inversion of the C3 carbon.

DISCUSSION

The design of peptidase inhibitors has been inspired by active site models since the mid 1970s when Ondetti and Cushman exploited knowledge of the carboxypeptidase A active site to design the ACE inhibitor captopril (Ondetti et al., 1977). In the 1980s James' group used an active site model derived from the coordinates of the metalloendopeptidase thermolysin to guide their neutral endopeptidase inhibitor design program (James et al., 1993). However, both the ACE and neutral endopeptidase active site models were based on the structures of distantly related peptidases since experimental models of the target enzymes were not available. Structural studies with truncated collagenase have thus provided the first zinc metalloproteinase X-ray coordinates which can be directly applied to drug design, and to our knowledge batimastat is the first metalloproteinase inhibitor to have entered clinical trials whose active site coordinates have been determined experimentally.

The role of the 2-thienylthiomethyl side chain on C3 is not entirely clear. Comparison of batimastat and structure **7** binding affinities (batimastat, 5 nM; **7**, 15 nM) shows that

Table 5: C-Terminal Hydroxamate Inhibitors Discussed in the Text[a]

no.	P1	P1′	P2′	P3′	ZBG	IC_{50} (HFC) (nM)
1 (BB-94)	2-ThiCH_2 (*S*)	CH_2-L-Leu	L-Phe	NHMe	HA	5
2	2-ThiCH_2 (*R*)	CH_2-D-Leu	L-Phe	NHMe	HA	2000
3	2-ThiCH_2 (*R*)	CH_2-D-Leu	D-Phe	NHMe	HA	inactive
4	Me (*S*)	CH_2-L-Leu	L-Tyr(OMe)	NHMe	HA	5
5	Me (*S*)	CH_2-D-Leu	L-Tyr(OMe)	NHMe	HA	4000
6	Me (*R*)	CH_2-L-Leu	L-Tyr(OMe)	NHMe	HA	50% at 10000
7	H	CH_2-L-Leu	L-Phe	NHMe	HA	15
8	H	CH_2-L-Leu	L-Tyr(OMe)	NHMe	CO_2H	30000

[a] Abbreviations: ZBG, zinc-binding group; HA, CONHOH; Thi, thiophene.

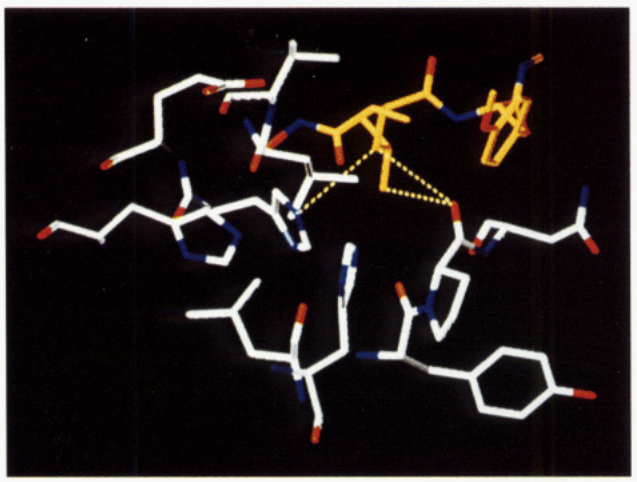

FIGURE 5: Illustration of the results of docking studies with structure **5**. Dotted lines in the figure highlight repulsive interactions between one of the inhibitor P1′ terminal methyl groups and the Pro217−Asn218 amide bond and between the displaced Cβ atom of the inhibitor leucine side chain and the Nϵ2 atom of the zinc-binding His197 residue. At the top of the figure is seen the Val194 residue whose favorable interaction with the terminal methyl groups of the P1′ Leu side chain is reduced by inversion at C2. Reading anticlockwise from the top left of the figure are seen residues Glu198, His201, Leu214, His207, Tyr216, Pro217, and Asn218. The carbon atoms of the inhibitor are colored orange.

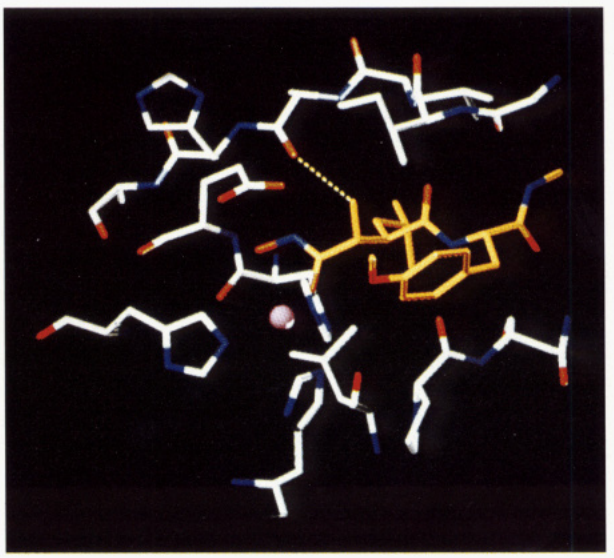

FIGURE 6: Illustration of the repulsive intermolecular interaction (dotted line) between the C3 methyl group of the inhibitor and the Ala161 carbonyl group, revealed by docking studies with structure **6**. At the top of the figure can be seen the β4 strand residues Ala163−Asn157. Below these residues lie the catalytic Glu198 residue, the three zinc-binding residues, His197 (background), His201 (left), and His207 (foreground). In the bottom right of the figure can be seen the proline turn residues Leu214, Pro217, and Asn218. The carbon atoms of the inhibitor are colored orange.

it contributes only modestly to binding affinity. Somewhat unexpectedly, the thiophene ring folds back over the N-terminal region of the inhibitor toward the hydroxamate group and does not occupy the cleft formed by the side chains of Ile159 and His162. In a similar fashion the P2′ Phe side chain points back toward the hydroxamic acid group shielding the inhibitor C3 atom from bulk solvent and does not lie in the Gly158−Ile159 cleft as might be expected (crystal contacts do not prohibit binding to this anticipated P2′ site). The compact batimastat conformation observed in the complex suggests that some of the binding energy may arise from favorable intramolecular interactions between the thiophene and phenyl rings. A similar clustering of hydrophobic groups has been found in X-ray crystal structures of thrombin complexes (Bode et al., 1990; Brandstetter et al., 1992; Lim et al., 1993). For the peptidic inhibitor PPACK, it has been shown that the hydrophobic packing found in the thrombin−PPACK complex is similar to the conformation found in solution (Lim et al., 1993) , and it is likely that the batimastat conformation observed in the complex is also present in solution.

The importance of zinc-binding groups for zinc metalloproteinase inhibition is well established and readily understood as arising from Coulombic attraction between an ionizable zinc-binding group and the positively charged Zn^{2+} ion. However, the question remains as to why the hydroxamate group should be so uniquely effective as a zinc-binding ligand. It is generally the case that hydroxamic acids give rise to more potent inhibitors than alternative zinc-binding groups such as carboxylic acids, thiols, or phosphinic acids (Beeley et al., 1994). Where the inhibitor is small and poor zinc binding is not compensated for by bulky groups elsewhere on the molecule, inhibitors with carboxylate zinc-binding groups are much less active than their hydroxamic acid analogues (compare structures **7** and **8**). Structural studies have revealed differences between hydroxamate− and carboxylate−ligand complexes which can explain at least some of the data obtained in *in vitro* studies. The zinc−oxygen distances observed on the batimastat−collagenase complex (average Zn−O distance = 2.1 Å) are shorter than those observed in an *N*-carboxymethyl-HFC−inhibitor complex (average Zn−O distance = 2.3 Å) (Lovejoy et al., 1994) and closer to those observed in unconstrained zinc−ligand complexes in the Cambridge Structural Database (average Zn - O distance = 2.04 ± 0.07 Å) (Hausin & Codin, 1990). In addition, the distance between the two zinc-binding oxygens on hydroxamic acids (2.7 Å) is greater than the corresponding distance on carboxylic acids (2.2 Å). As a consequence, hydroxamic acids are able to approach closer than carboxylic acids to the trigonal-bipyramidal geometry

predicted by ligand field theory to be required for optimal zinc binding. Finally, hydroxamic acids have pK_a values around 8.5 and in contrast to phosphinic acids and carboxylic acids exist as un-ionized neutral species at physiological pH. Mechanistic studies with hydroxamate TLN inhibitors have shown that they bind to the active site as the neutral species and that ionization follows rather than proceeds the initial binding step (Izquierdo-Martin & Stein, 1992). The contribution to the free energy of binding arising from desolvation of the inhibitor will therefore favor hydroxamic acids over charged zinc-binding groups such as carboxylic acids and phosphinic acids. Indeed, solvation energy may be the major factor differentiating the zinc-binding properties of neutral zinc-binding groups such as thiols and hydroxamic acids from charged groups such as carboxylic and phosphinic acids.

Collagenase structural studies show that all substrate-like right-hand-side inhibitors published to date adopt a common binding mode with the P1′ group fitting in the S1′ pocket and virtually identical inhibitor−enzyme backbone interactions. In a similar fashion crystallographic studies have shown that TLN inhibitors adopt a single conformation in the active site (Matthews, 1988). Modeling studies with ACE inhibitors have also shown that, in spite of their structural heterogeneity, they can be superimposed on a single pharmacophore (Mayer et al., 1987; Hangauer, 1989), and it is probable that they adopt a single orientation in the active site. The absense of alternative binding modes observed with zinc metalloproteinase−inhibitor complexes can be attributed to the strongly directional zinc binding and backbone−backbone interactions between the inhibitor and the active site. Just as early molecular modeling studies with ACE inhibitors profited from the fact that these inhibitors can be superimposed on a common pharmacophore, the absense of multiple binding modes observed with MMP inhibitors should simplify the task confronting drug design groups aiming to exploit MMP coordinates to improve inhibitor potency or selectivity.

ACKNOWLEDGMENT

We thank Prof. R. Huber for continuous support, the British Biotech enzyme assay group for carrying out the MMP IC_{50} determinations, Bhavesh Mistry for assisting with the molecular modeling calculations, and Paul Beckett, Andy Miller, and Mark Whittaker for useful discussions. The financial support of the Sonderforschungsbereiche 207 (W.B.) and 237 (H.T.) and of the Fonds der Chemischen Industrie (W.B. and H.T.) is gratefully acknowledged.

REFERENCES

Abramson, M., Schilling, R. W., Huang, C.-C., & Salome, R. G. (1975) *Ann. Otol., Rhinol., Laryngol. 84*, 158−163.

Alabaster, E. T., Barclay, P. L., Barnish, I. T., Blackburn, K. J., Brown, D., Campbell, S. F., Cussans, N. J., Danilewicz, J. C., Palmer, M. J., Samuels, G. M. R., Terrett, N. K., & Wythes, M. J. (1993) in *Perspectives in Medicinal Chemistry* (Fuhrer, W., Giger, R., Kyburz, E., & Testa, B., Eds.) Chapter 4 pp 45−60, Verlag Helvitica Chimica Acta, Basel, Switzerland.

Allen, F. H., & Kennard, O. (1993) *Chemical Des. Autom. News 8*, 31−37.

Beeley, N. R. A., Ansell, P. R. J., & Docherty, A. J. P. (1994) *Curr. Opin. Ther. Pat. 4*, 7−17.

Bode, W., Turk, D., & Sturzebecher, J. (1990) *Eur. J. Biochem. 193*, 175−182.

Bode, W., Gomis-Rüth, F.-X., & Stöcker, W. (1993) *FEBS Lett. 331*, 134−140.

Bode, W., Reinemer, P., Huber, R., Kleine, T., Schnierer, S., & Tschesche, H. (1994) *EMBO J.* 1263−1269.

Borkakoti, N., Winkler, F. K., Williams, D. H., D'arcy, A., Broadhurst, M. J., Brown, P. A., Johnson, W. H., & Murray, E. J. (1994) *Struct. Biol. 1*, 106−110.

Brandstetter, H., Turk, D., Hoeffken, H. W., Grosse, D., Sturzebecher, J., Martin, P. D., Edwards, B. F., & Bode, W. (1992) *J. Mol. Biol. 226*, 1085−1099.

Brown, P. D. (1993) *Curr. Opin. Invest. Drugs 2* (6), 617−626.

Brünger, A. T. (1993) *X-PLOR Version 3.1 Manual*, Yale University, New Haven, CT.

Campion, C., Davidson, A. H., Dickens, J. P., & Crimmin, M. J. (1990) WO Patent 90/05719.

Cawston, T. E., & Barrett, A. J. (1979) *Anal. Biochem. 99*, 340−345.

Davies, B., Brown, P. D., East, N., Crimmin, M. J., & Blackwill, F. R. (1993) *Cancer Res. 53*, 2087−2091.

D'Errico A., Garbisa, S., Liotta, L. A., Castronovo, V., Stetler-Stevenson, W. G., & Grigioni, W. F. (1991) *Mod. Pathol. 4*, 239−246.

Docherty, A. J. P., Lyons, A., Smith, B. J., Wright, E. M., Stephens, P. E., Harris, T. J. R., Murphy, G., & Reynolds, J. J. (1985) *Nature 38*, 66−69.

Engh, R. A., & Huber, R. (1991) *Acta Crystallogr., Sect. A 47*, 392−400.

Grams, F., Reinemer, P., Powers, J. E., Kleine, T., Pieper, M., Tschesche, H., Huber, R., & Bode, W. (1995) *Eur. J. Biochem. 228*, 830−841.

Grams, F. (1995) Strukturbasierendes Wirkstaff-design an Metalloproteasen, Ph.D. Thesis, Technische Universitat, Munich.

Hangauer, D. G. (1989) in *Computer-Aided Design and Evaluation of Angiotensin-Converting Enzyme Inhibitors* (Perun, T. J., & Propst, C. L., Eds.) pp 253−295, Marcel Decker Inc., New York.

Hasty, K. A., Reife, R. A., Kang, A. H., & Stuart, J. M. (1990a) *Arthritis Rheum. 33*, 388−397.

Hasty, K. A., Pourmotabbed, T. F., Goldberg., G. I., Thompson, J. P., Spinelle, T. G., Stephens, R. M., & Mainardi, C. L. (1990b) *J. Biol. Chem. 265*, 11421−11421.

Hausin, R. J., & Codding, P. W. (1990) *J. Med. Chem. 33*, 1940−1947.

Insight II, Version 2.2.0 (1993) Biosym Technologies, San Diego.

Izquierdo-Martin, M., & Stein, R. L. (1992) *J. Am. Chem. Soc. 114*, 325−331.

Jones, T. A. (1978) *J. Appl. Crystallogr. 15*, 23−31.

Krutzsch, H. E., Liotta, L. A., & Stetler-Stephenson, W. G. (1989) *J. Biol. Chem. 264*, 17374−17378.

Kubocki, K. (1990) *Nippon Geka Gakkai Zasshi 91*, 174−183.

Leslie, A. G. W. (1991) *Daresbury Lab. Inf. Q. Prog. Crystallogr. 26*, available from the Librarian, SERC Laboratory, Daresbury, Warrington, WA4 4AD, U.K.

Lim, M. S., Johnston, E. R., & Kettner, C. A. (1993) *J. Med. Chem. 36*, 1831−1838.

Lovejoy, B., Cleasby, A., Hassell, A. M., Longley, K., Luther, M. A., Weigl, D., McGeehan, G., McElroy, A. B., Drewry, D., Lambert, M. H., & Jordan, S. R. (1994) *Science 263*, 375−377.

Matthews, B. W. (1988) *Acc. Chem. Res. 21*, 333−340.

Mayer, D., Naylor, E. B., Motoc, I., & Marshall, G. R. (1987) *J. Comput.-Aided Mol. Des. 1*, 3−16.

McCachren, S. S., Haynes B. F., & Niedel, J. E. (1990) *J. Clin. Immunol. 10*, 19−27.

Muller, D., Breathnach, R., Engelmann, A., Millon, R., Bronner, G., Flesch, Dumont, P., Eeber, M., & Abecassis, J. (1991) *Int. J. Cancer 48*, 550−556.

Ondetti, M. A., Rubin, B., & Cushman, D. W. (1977) *Science 196*, 441−444.

Pavloff, N., Staskus, P. W., Kishnani, N. S., & Hawkes, S. P. (1992) *J. Biol. Chem. 267*, 17321−17326.

Reinemer, P., Grams, F., Huber, R., Kleine, T., Schnierer, S., Piper, M., Tschesche, H., & Bode, W. (1994) *FEBS Lett. 338*, 227−233.

Schnierer, S., Kleine, T., Gote, T., Hillemann, A., Knäuper, V., & Tschesche, H. (1993) *Biochem. Biophys. Res. Commun. 191*, 319−326.

Spurlino, J. C., Smallwood, A. M., Carlton, D. D., Banks, T. M., Vavra, K. J., Johnson, J. S., Cook, E. R., Falvo, J., Wahl, R. E., Pulvino, T. A., Wendoloski, J. J., & Smith, D. L. (1994) *Proteins 19*, 98−109.

Stack, S. M., & Gray, R. D. (1989) *J. Biol. Chem. 264*, 4277−4281.

Stams, T., Spurlino, J. E., Smith, D. L., Wahl, R. E., Qoronfleh, M. W., Banks, T. M., & Rubin, B. (1994) *Struct. Biol. 1* (2), 119−123.

Steigemann, W. (1991) in *From Chemistry to Biology* (Moras, D., Podjarny, A. D., & Thierry, J. C., Eds.) *Crystallographic Computing*, Vol. 5, pp 115−125, Oxford University Press, Oxford, U.K.

Stewart, J. J. P. (1990) *J. Comput.-Aided. Mol. Des. 4*, 1−105.

SYBYL Version 6.1 (1995) TRIPOS Associates, 1699 South Hanley Road, Suite 303, St. Louis, MO 6314.

Weiner, S. J., Kollman P. A., Case, D. A., Chandra Singh, U., Ghio, C., Alagona, G., Profeta, J. R. S., & Weiner, P. (1984) *J. Am. Chem. Soc. 106*, 765−784.

BI951203G